

The Structure of an Open Form of an *E. coli* Mechanosensitive Channel at 3.45 Å Resolution

Wenjia Wang,^{1*} Susan S. Black,^{2*} Michelle D. Edwards,^{2*} Samantha Miller,² Emma L. Morrison,² Wendy Bartlett,² Changjiang Dong,¹ James H. Naismith,^{1†} Ian R. Booth^{2†}

How ion channels are gated to regulate ion flux in and out of cells is the subject of intense interest. The *Escherichia coli* mechanosensitive channel, MscS, opens to allow rapid ion efflux, relieving the turgor pressure that would otherwise destroy the cell. We present a 3.45 angstrom-resolution structure for the MscS channel in an open conformation. This structure has a pore diameter of ~13 angstroms created by substantial rotational rearrangement of the three transmembrane helices. The structure suggests a molecular mechanism that underlies MscS gating and its decay of conductivity during prolonged activation. Support for this mechanism is provided by single-channel analysis of mutants with altered gating characteristics.

Ion channels display two intrinsic properties: selectivity and gating in response to specific stimuli. Despite extensive study, the structural changes that accompany the gating transition from closed (nonconducting) to open (conducting) states are poorly understood for many channels. Bacterial channels have proved to be excellent experimental systems for analysis and have provided invaluable insights into all facets of channel biology (1–6). The bacterial mechanosensitive channels, MscS and MscL, open in response to membrane tension so that small osmotically active ions and molecules can exit the cell (6, 7), allowing bacteria to survive hypo-osmotic shocks equivalent to transmembrane pressures ≥ 14 atm (8). The free energy required to open these channels is relatively small, ~28 kJ/mol and ~46 kJ/mol for MscS and MscL, respectively (9, 10).

MscS and MscL have been characterized in detail, including characterization by three-dimensional crystallographic analysis (7, 11, 12). The crystal structure of MscL has been determined in a nonconducting state (7, 11). The first crystal structure for MscS revealed the protein was a heptamer with a sevenfold rotational axis parallel to the normal axis of the membrane (11). Each monomer has three N-terminal transmembrane helices; these are named TM1 (residues 30 to 50), TM2 (residues 60 to 90), and TM3 (residues 95 to 126) (11, 13). A pronounced kink centered at G113 (14) separates TM3 into the pore-lining TM3a helix (S95 to L111) and the TM3b helix (G113 to M126), which connects to the C-terminal domain. Seven TM3a helices are arranged in a helical barrel, the central axis of

which marks out the presumed route of ions across the membrane. The seven TM3b helices point outwards from the central barrel tangential to the pore axis. The cytoplasmic C-terminal domains from each monomer are assembled by the sevenfold symmetry into an oval-shaped compartment with a large central cavity that is contiguous with the TM3a helical barrel (11). Entrance to the central cavity is through seven 10-by-8 Å portals arranged around the side of the oval. The original crystal structure was assigned as an open form (11). However, subsequent analysis and modeling established that the structure represents a nonconducting state (15). In the closed form, the side chains of L105 and L109 are inserted into the pore lumen. These two rings of bulky hydrophobic side chains and the hydrophobic nature of TM3a have been proposed to prevent wetting of the channel pore, thus blocking the passage of ions, including the hydronium ion; this has been termed a “vapor lock” (15, 16).

A conserved pattern of glycine and alanine residues in TM3a of MscS (termed “knobs and holes”) is important in gating and also in forming the tightly packed, symmetrical TM3a arrangement seen in the nonconducting form (17). As part of this investigation, we identified A106V as one of a series of mutants with unique electrophysiological properties in vitro that are sufficiently distinct from the wild type to allow us to generate new crystallographic insights. Crucially, the mutant is fully functional in vivo (17). Here we report the crystal structure of an open/conducting form of MscS and propose a structural model for the transition from the closed to the open state. Crystal structures are necessarily static structures, and there may be additional open and/or closed states in vivo. We have therefore supported our model by testing its predictions with an analysis of mutants created by site-directed mutagenesis.

A106V structure. The A106V protein assembles in the membrane, protects in hypo-osmotic

shock assays, and gates at pressures intermediate between wild type (WT) MscS and MscL (fig. S1) (17, 18). The principal distinctions of the mutant are its increased resistance to pressure and ability to adopt a reduced-conducting state at high pressures. Overall, therefore, the mutation by itself does not grossly change protein activity in vivo. MscS A106V was crystallized following the same protocol developed for WT MscS (11), and the structure was solved using molecular replacement to 3.45 Å resolution. The transmembrane helices were removed from the molecular-replacement model and fitted to unbiased difference electron density (19). A106V MscS is a heptamer and, like the WT structure, is composed of three cytoplasmic domains and a transmembrane region of three helices (Fig. 1, A and B). The cytoplasmic portion is essentially unchanged from the wild type (7, 11), but there are major changes in the transmembrane domain (Fig. 1B). On the basis of these differences, we identify the A106V structure as an open/conducting state of MscS, in contrast to a closed/nonconducting form seen in the WT protein crystal structure. In the wild type, nonconducting structure, A106 is packed against G108 from the neighboring subunit so that structural rearrangement would be required to accommodate a valine side chain (fig. S2A). We suggest that it is the additional bulk of 106V that hinders formation of the state previously observed in the WT crystals (11).

Pronounced changes in transmembrane region. Relative to the closed structure, TM1 and TM2 rotate as a rigid unit by ~45° clockwise (Fig. 1B and fig. S3) (20). In addition to the rotation, TM1 and TM2 helices increase their tilt by 15° with respect to the sevenfold axis. This motion results in their burying more volume in the membrane. The loop between TM1 and TM2 now interacts with the surface of TM3b within the same monomer and with TM3a of the neighboring monomer (fig. S2B). We suggest that it is these specific interactions that stabilize the state we observe. Importantly, these interactions are all remote from the A106V mutation, and 106V occupies a large open pocket (fig. S2B). Thus, although the A106V mutation has enabled an open form to be trapped, we do not believe that the side chain has created an artefactual open state.

Accompanying the changes in TM1 and TM2, TM3a pivots around the C α of G113 (Fig. 1C). TM3b, which is attached to the cytoplasmic domain, remains essentially unchanged. In the mutant, the TM3a helices have moved outwards from the central axis and have rotated around their axis by ~15° clockwise (Figs. 1C and 2A). At the N-terminal end of TM3a, the C α of S95 shifts by over 9 Å and at the C-terminal end, the C α of L109 moves by ~4 Å. In permitting this movement of TM3a, G113 does not adopt Ramachandran angles forbidden to other amino acids, consistent with both its lack of conservation in other MscS proteins and its insensitivity to mutation in *Escherichia coli* (21, 22). It has been proposed that during the

¹Centre for Biomolecular Sciences, The North Haugh, University of St. Andrews, KY16 9ST, Scotland, UK. ²School of Medical Sciences, Institute of Medical Sciences, University of Aberdeen, Foresterhill, Aberdeen, AB25 2ZD, Scotland, UK.

*These authors contributed equally to this work.

†To whom correspondence should be addressed. E-mail: naismith@st-and.ac.uk (J.H.N.); i.r.booth@abdn.ac.uk (I.R.B.)

opening of the channel, TM3a lengthens and TM3b shortens, such that the junction between TM3a and TM3b moves from G113 to G121 (27). The struc-

tural conservation of the TM3a to TM3b junction in the mutant and WT crystal structures does not support this hypothesis.

An open structure for MscS. In the open structure, the helical axes of the seven TM3a helices are parallel to each other, to the sevenfold axis, and

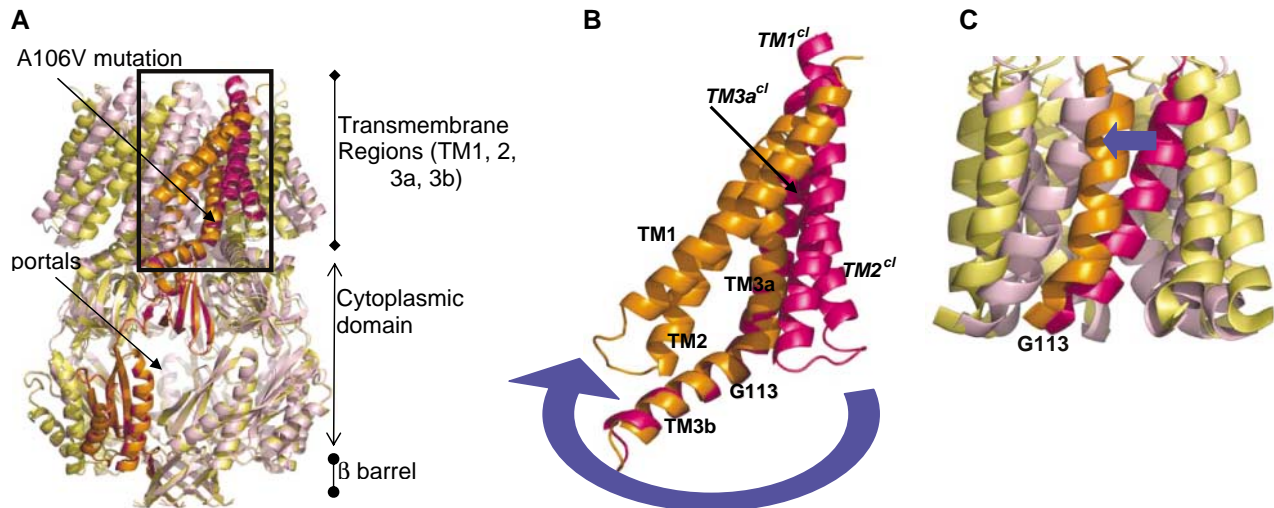


Fig. 1. Conformation changes between the A106V and WT structures. **(A)** Structures are orientated such that the sevenfold axis is parallel to the membrane normal. For the A106V structure, one monomer (subunit A) is colored orange; the remaining six subunits B to G are shown in gold. The site of the A106V mutation is highlighted. For the WT structure, the A subunit is colored purple, and the remaining six subunits B to G are shown in lilac. One of the seven portals through which ions are presumed to enter from the cytoplasm is marked. The cytoplasmic domain is essentially unchanged from the WT structure; however, there are profound changes in the transmembrane helices, which are boxed. An orthogonal view is shown in fig. S3. The environments of A106 and 106V in their respective structures are shown in more detail in fig. S2. **(B)** Expanded view of the boxed transmembrane helices of

the A subunit. The helices are colored and oriented as above. The blue arrow represents the motion from the closed to the open state. The helices are labeled TM1, 2, 3a, and 3b in accordance with the text. In the A106V structure, TM1 and TM2 have undergone a rigid-body clockwise rotation relative to their position in the closed structure (labeled $TM1^{cl}$ and $TM2^{cl}$). TM3a also adjusts its position relative to the closed form ($TM3a^{cl}$). There is only a small change in TM3b. G113, the pivot point, is labeled. **(C)** Central pore showing only TM3a colored and oriented as in (A). Comparing the WT and A106V channel structures, TM3a has pivoted around G113. The blue arrow denotes the movement from closed to open states. As a result of this motion, the helical axis of TM3a in the A106V structure is parallel to the membrane normal, rather than at an angle as in the WT structure.

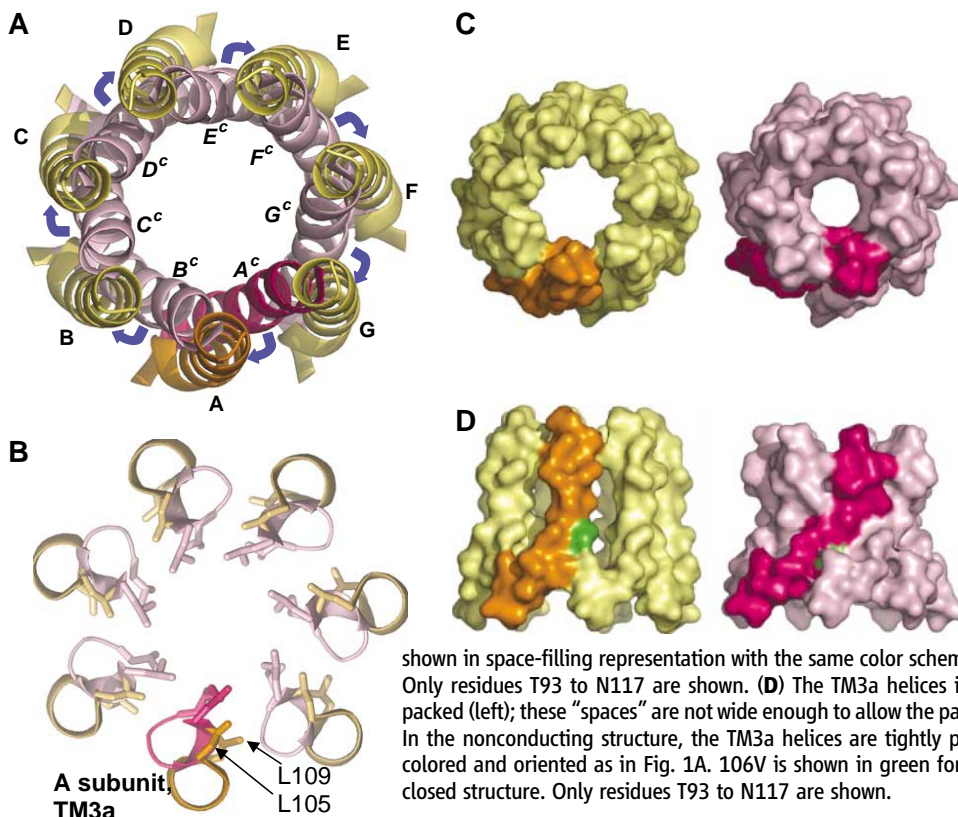


Fig. 2. A106V represents an open structure. **(A)** Superposition of the helical pore (helix TM3a) in MscS. The color scheme is the same as in Fig. 1A. The subunits are labeled; the labels for those in the closed structure are on the inside. The TM3a helices in the A106V MscS structure move out from the center and align parallel to the sevenfold axis. The blue arrows denote motion from the closed to the open state. The helical pore is oriented such that one is looking from the periplasm into the cytoplasm. **(B)** The L105 and L109 side chains, which fill the central pore in closed structure, have moved out of the pore in the A106V structure, creating the open channel by breaking the vapor lock. This motion is akin to the opening of camera iris. The color scheme is the same as in Fig. 1A and the orientation as in (A). **(C)** The pore formed by the seven TM3a helices in the A106V MscS (left) has a diameter of ~ 13 Å and is assigned as an open (conducting) state of MscS. The WT channel has a diameter of 4.8 Å (right) and is thought to represent a closed (nonconducting) channel. The TM3a helices are shown in space-filling representation with the same color scheme as in Fig. 1A and the same orientation as in (A). Only residues T93 to N117 are shown. **(D)** The TM3a helices in the conducting A106V structure are not tightly packed (left); these "spaces" are not wide enough to allow the passage of molecules but may interact with the lipids. In the nonconducting structure, the TM3a helices are tightly packed (right). The open and closed structures are colored and oriented as in Fig. 1A. 106V is shown in green for the open structure, and A106 is in green for the closed structure. Only residues T93 to N117 are shown.

to the membrane normal (Fig. 1C). This is quite distinct from the arrangement seen in the closed structure, where TM3a helices are diagonal to the sevenfold axis. The interior of the pore remains predominantly hydrophobic, as the main-chain atoms are all involved in helical interactions and do not present a polar surface. However, we cannot experimentally determine the extent of TM3a solvation. As a result of these changes in TM3a, the

side chains of L105 and L109 have moved out from the center of the pore in the A106V mutant structure, in a manner reminiscent of the plates of a mechanical camera iris (Fig. 2B). This breaks the vapor lock by expansion of the pore, a mechanism suggested from the modeling of nanotubes (16). We expect that this represents an open channel rather than a subconducting state, because the A106V mutant channel only forms subconduct-

ing states when subjected to high tension close to that required to open MscL. Such conditions are unlikely to prevail in protein crystals.

The program HOLE (23) estimates that the pore in the open structure has a diameter of just under 13 Å, as compared with 4.8 Å for the closed structure (7, 11) (Fig. 2C). At 13 Å, this is very clearly conducting and would allow the passage of solvated ions and small solutes. The outer membrane protein Wza, which allows the passage of complex oligosaccharides, has a helical barrel with a comparable internal diameter of 17 Å (24). The increase in diameter of 8 Å is similar to that previously predicted (9). The central pore in the A106V structure is now wider than the lateral cytoplasmic portals and suggests that it is the flow into the cytoplasmic central cavity through the portals, not out through the TM3a pore, that limits the observed conductivity to 1200 pS (where $1 \text{ S} = 1 \text{ A/V}$) (9, 10). This is consistent with the increased conductivity observed for a deletion mutant lacking the base of MscS, consequently creating a larger opening into the central cytoplasmic cavity (Fig. 1A) (22).

The A110-115 "switch." The change in position of TM3a with respect to TM3b is accompanied by a shift of A110 (TM3a) from one side of the L115 side chain (TM3b) of a neighboring monomer to the other side (Fig. 3A). Analogous to a switch, we believe this interaction defines an open and closed state of the channel. Because the open state is higher in energy, this switch will stabilize the open form by creating a kinetic barrier. To test this hypothesis, mutations were introduced: A110 to G and V and L115 to G, I, and V. All of the mutant proteins were inserted into the membrane at levels comparable to the wild type (fig. S4). An A110V mutant is extremely difficult to open [$P_L:P_S \sim 1.08 \pm 0.04$; $\sim 42 \text{ kJ/mol}$ (25) as compared with $P_L:P_S \sim 1.59$; 28.4 kJ/mol for WT MscS], exhibits reduced conductance (17), and does not protect against osmotic downshock (fig. S1). The A110G mutant protects against downshock but opens at lower pressures than does the wild type ($P_L:P_S \sim 2.2$; $\sim 20 \text{ kJ/mol}$) and is unstable in the open state (Fig. 4 and fig. S1). L115V also protects against downshock and opens at lower pressures than does the wild type ($P_L:P_S \sim 2.1$; $\sim 22 \text{ kJ/mol}$), though its behavior was complex (Fig. 4B and fig. S1). These observations are consistent with our model, which suggests that the bulkier A110V would require more structural distortion to go past L115. In contrast, the A110G and L115V mutants having smaller side chains at these positions, would allow easier interconversion between closed and open states, and thus open at a lower pressure and create flickery channel behavior (Fig. 4).

Functional analysis of the gating transitions. In the gating transition, the methyl group of A102 has to slide across the protein surface of TM3a from the neighboring subunit (Fig. 3B). This would represent an obstacle to closure that could stabilize the open form. We created single mutants at A102 to test this and extend our analysis of TM3a (17) (fig. S1). An A102G mutant opened at a similar pressure to that of the wild type ($P_L:P_S$

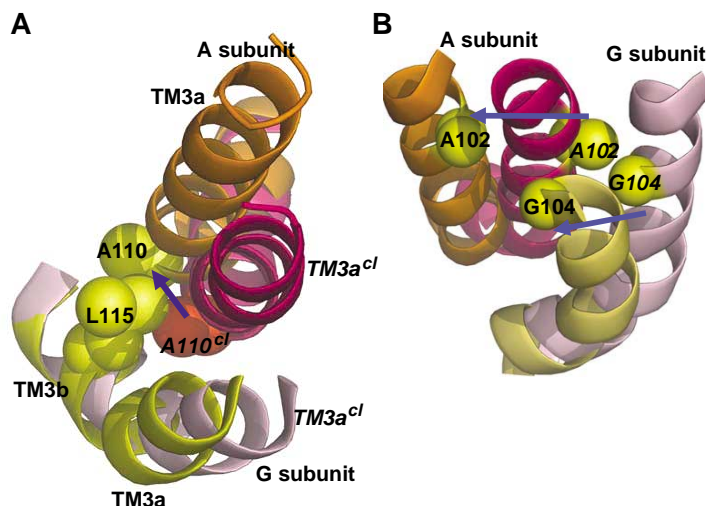
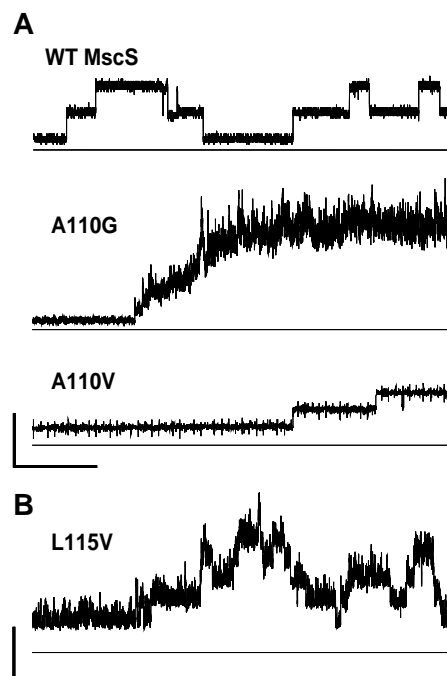


Fig. 3. Structural features of the channel transition. (A) In the closed structure, the side chain of A110 (shown as a red sphere) sits in a pocket on one side of the L115 side chain in TM3b from the neighboring G subunit. In the open A106V structure, A110 (shown as a yellow sphere) sits in another pocket on the opposite side of the L115 side chain. These different positions of A110, akin to a switch, define the closed and open states. The remainder of the molecule is colored as in Fig. 1A. The blue arrow defines the motion from closed to open. (B) The methyl group of A102 from the A subunit must cross the face of TM3a from the G subunit, creating a guide to the opening and closing. The A102G mutant opens and closes more easily than the WT channel, consistent with the removal of this guide. The double mutant A102G/G104A reintroduces a methyl group, re-creating the guide, and is indeed essentially WT. The molecules are colored the same as in Fig. 1A.

Fig. 4. Mutations at A110 and L115 affect MscS channel opening. Patch clamp analysis of excised protoplast membrane patches expressing WT or mutant MscS protein. (A) WT channels show step-like opening and closing events. Substitution of A110 to glycine produces channels that are unstable in the open state; thus openings are rapidly followed by closures giving channel activity of a flickery appearance. Substitution to valine leads to a channel that does not open fully; its open state is stable but exhibits a decreased conductance. (B) Exchange of L115 for a smaller valine residue disrupts the ability of the channel to open fully and/or remain open. Vertical scale bar, 50 pA; horizontal scale bar, 200 ms.



$\sim 1.54 \pm 0.11$; ~ 29 kJ/mol) but was unable to sustain the fully open state (Fig. 5A). The A102G mutant exhibited a flickery channel phenotype that undergoes rapid adaptation (Fig. 5B). This is consistent with a model in which the loss of the methyl group reduces the barrier between the states and allows very rapid cycling between them once sufficient pressure is applied to gate the channel. An A102V mutation significantly increased the pressure to gate the channel ($P_L:P_S \sim 1.26 \pm 0.04$; ~ 36 kJ/mol) (fig. S1), presumably because the bulkier valine side chain cannot easily slide across the surface.

Single-mutant analysis can prove misleading, as changing one residue may modify a number of interactions, and this may have the consequence of potentiating kinetic pathways that are cryptic in the WT protein (26). To further test our model, we sought to identify residues that couple with A102G using mutant cycle analysis, which has proved invaluable in both enzymology and the study of ion channels (26–30). A second mutation was introduced either at G104, a position the model suggests should be coupled, or at G101, which the model predicts is not coupled. The A102G/G104A double mutant exhibited both a WT gating pressure ($P_L:P_S \sim 1.50 \pm 0.02$; ~ 30 kJ/mol) and a stable open state (Fig. 5C and fig. S1). Pressure-difference calculations for this mutant cycle were greater than zero (0.38), indicating coupling between the two residues (Fig. 5D) (26, 29–31).

Fig. 5. Alanine at position 102 is important to maintain the open state of MscS. (A to C) Patch clamp recordings of WT and A102G mutant MscS channels. (A) A102G mutation renders the channels unstable in the open state. Vertical scale bar, 50 pA; horizontal scale bar, 200 ms. (B) Prolonged application of pressure (shown in lower panel of both traces) causes open WT channels to adapt and become nonconducting. Thus, the current trace (upper panel in each recording) returns to baseline in the presence of applied pressure. A102G mutant channels rapidly adapt to sustained pressure. Vertical scale bar, 200 pA and 340 mmHg; horizontal scale bar, 10 s. (C) Reciprocal double mutations at positions 102/101 or 102/104 return the stable, fully open conformation. Vertical scale bar, 50 pA; horizontal scale bar, 200 ms. (D) Mutant cycle analysis (26) of the gating pressures (derived from patch clamp analysis) for each single and double mutant. The $P_L:P_S$ ratio for each single and double mutant was measured as described in the SOM (18). The $P_L:P_S$ ratio difference between the single mutants and the wild type, and between double mutants and single mutants, was calculated to measure the change associated with the introduction of the indicated mutation. Summation across the diagram (i.e., comparing the effect of introducing a specific mutation into either the WT or mutant channel) indicates that, whereas residue G101 does not couple to A102 (difference value of 0.02 is close to zero), G104 and A102 appear to energetically interact (difference value of 0.38 is greater than zero) (26–31).

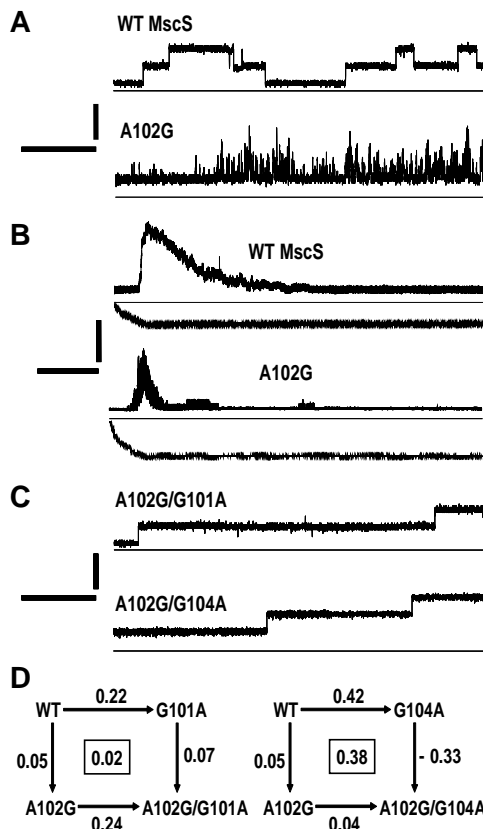
The double mutant A102G/G104A reintroduces a methyl group (in TM3a from the neighboring subunit) opposite A102G (Fig. 3B). Our model had suggested that this reintroduction of the methyl group would re-create the kinetic barrier of a methyl group moving across a protein surface (Fig. 5), and this appears to be the case. In contrast, the G101A/A102G double mutant exhibited stable channel openings, but the pressure required for opening was the same as that for the G101A single mutant alone ($P_L:P_S \sim 1.37 \pm 0.05$; ~ 33 kJ/mol) (Fig. 5C and fig. S1). The calculated pressure difference for the mutant cycle was close to zero (0.02; Fig. 5D), supporting our structural model, which suggests the independence of these two residues (30, 31).

A molecular model for adaptation. During sustained application of subsaturating pressures to membrane patches, *E. coli* MscS channels will decay to a nonconducting state; this is termed “adaptation” (1, 8, 21, 22, 32). Adaptation has two contributory processes: inactivation and desensitization. Inactivated channels can be reactivated after resting in the absence of pressure (21), whereas desensitized channels can be reactivated by increasing the pressure. These processes are common in many channels and receptors (33), yet structural understanding is sparse. In this open form of MscS, the seven TM3a helices are no longer close-packed but are physically separated (Fig. 2D). In returning to the closed form, the very specific pattern of knobs and holes of TM3a must

be re-established. There is the possibility that during this “repacking” the protein molecule could become conformationally trapped by mismatching the knobs and holes. The rate of adaptation would then be proportional to the rate of cycling between open and closed states. This is indeed the case: At pressures high above the gating threshold, where the channel is open with no cycling between states, no decay is observed. The mutant A102G, which rapidly flickers between open and closed states, exhibits very rapid adaptation (Fig. 5B). Changes that increase the separation between TM3a helices are predicted by our model to lead to more rapid adaptation. In both structures Q112 points into the pore and in the closed form makes contacts with several other residues. The Q112G mutant that would remove this “guiding hand,” shows an extremely rapid decay of conductivity (21). Because MscK (an *E. coli* homolog of MscS) has much bulkier side chains in TM3a, one might predict a more constrained pathway to the closed state. Indeed, MscK does not exhibit any decay of conductivity (8). Rapidly adapting MscS mutants have been described with changes that are located in TM3b and in the loop between TM1 and TM2 (21, 34). Our model suggests that these mutations perturb protein/protein interactions, as TM1-TM2 crosses the face of TM3b (Fig. 1B) during the transition between states.

Model for channel gating. The rearrangement of the three transmembrane helices between the closed and open conformations of MscS presents a structural basis on which we can now propose a molecular model for channel gating. Under excessive outwardly directed turgor pressure, the density of lipids in the cytoplasmic membrane is decreased. TM1 and TM2 respond to this decrease in density by adjusting their conformation to increase their buried volume. We suggest that the rotation and tilting movement of TM1 and TM2 act as a lever on TM3a. This rigid-body movement of TM1-TM2 is conceptually similar to the movement of the “voltage sensing paddle” in the voltage-dependent potassium channel KvAP (35–38). TM3a then pivots around Q112 to G113 while the rest of the structure remains essentially unchanged. This movement of TM3a withdraws the side chains of L105 and L109 from the central pore, breaking the vapor lock and allowing solvated ion transport (Fig. 2). Leucine rings are a central motif in many channels, and mutational analysis has shown similar roles to those proposed for MscS (39–41). The tight packing of these leucine residues in the closed form is important for protein stability and function. Single mutants of L105 or L109 to smaller amino acids affect the assembly of the channel in the membrane (42). Notably, the channels that do form still gate but at lower pressures, suggesting that one leucine ring alone can block conduction. This is analogous to mutants affecting the leucine rings in the acetylcholine receptor that lower the concentration of agonist required to gate the channel (40, 41).

The opening and closing of channels is central to biology, yet is still poorly understood at a mo-



lecular level. The use of mutants with modified gating kinetics may prove a widely applicable approach to crystallize different channel conformations. By combining functional data with an open structure of the MscS channel, we have described the transitions between closed and open forms that involve tilting and separation of the transmembrane helices reminiscent of a camera iris.

References and Notes

- B. Akitake, A. Anishkin, S. Sukharev, *J. Gen. Physiol.* **125**, 143 (2005).
- I. R. Booth, M. D. Edwards, S. Miller, *Biochemistry* **42**, 10045 (2003).
- R. Dutzler, E. B. Campbell, M. Cadene, B. T. Chait, R. MacKinnon, *Nature* **415**, 287 (2002).
- Y. Jiang *et al.*, *Nature* **417**, 515 (2002).
- Y. Jiang *et al.*, *Nature* **417**, 523 (2002).
- C. Kung, *Nature* **436**, 647 (2005).
- S. Steinbacher, R. Bass, P. Strop, D. C. Rees, *Curr. Top. Membr.* **58**, 1 (2007).
- N. Levina *et al.*, *EMBO J.* **18**, 1730 (1999).
- S. Sukharev, *Biophys. J.* **83**, 290 (2002).
- S. I. Sukharev, W. J. Sigurdson, C. Kung, F. Sachs, *J. Gen. Physiol.* **113**, 525 (1999).
- R. B. Bass, P. Strop, M. Barclay, D. C. Rees, *Science* **298**, 1582 (2002).
- G. Chang, R. H. Spencer, A. T. Lee, M. T. Barclay, D. C. Rees, *Science* **282**, 2220 (1998).
- S. Miller, M. D. Edwards, C. Ozdemir, I. R. Booth, *J. Biol. Chem.* **278**, 32246 (2003).
- Single-letter abbreviations for the amino acid residues are as follows: A, Ala; C, Cys; D, Asp; E, Glu; F, Phe; G, Gly; H, His; I, Ile; K, Lys; L, Leu; M, Met; N, Asn; P, Pro; Q, Gln; R, Arg; S, Ser; T, Thr; V, Val; W, Trp; and Y, Tyr.
- A. Anishkin, S. Sukharev, *Biophys. J.* **86**, 2883 (2004).
- O. Beckstein, M. S. P. Sansom, *Proc. Natl. Acad. Sci. U.S.A.* **100**, 7063 (2003).
- M. D. Edwards *et al.*, *Nat. Struct. Mol. Biol.* **12**, 113 (2005).
- Pressure ratios were measured using the patch clamp technique, and experimental details are reported in the supporting online material (SOM) and in fig. S1.
- Extensive details of the crystallography are given in the SOM and in fig. S5.
- Clockwise is defined when looking along the sevenfold axis from the periplasm into the cytoplasm.
- B. Akitake, A. Anishkin, N. Liu, S. Sukharev, *Nat. Struct. Mol. Biol.* **14**, 1141 (2007).
- M. D. Edwards, W. Bartlett, I. R. Booth, *Biophys. J.* **94**, 3003 (2008).
- O. S. Smart, J. G. Neduvetil, X. Wang, B. A. Wallace, M. S. P. Sansom, *J. Mol. Graphics* **14**, 354 (1996).
- C. Dong *et al.*, *Nature* **444**, 226 (2006).
- The value for the free energy change reported for the mutants is calculated by proportionation, assuming a linear relation between the free energies of the closed-to-open transitions of MscS and of MscL. Our interpretation does not depend on this linearity.
- L. Serrano, A. Horovitz, B. Avron, M. Bycroft, A. R. Fersht, *Biochemistry* **29**, 9343 (1990).
- J. Aiyar, J. P. Rizzi, G. A. Gutman, K. G. Chandy, *J. Biol. Chem.* **271**, 31013 (1996).
- R. Ranganathan, J. H. Lewis, R. MacKinnon, *Neuron* **16**, 131 (1996).
- P. J. Carter, G. Winter, A. J. Wilkinson, A. R. Fersht, *Cell* **38**, 835 (1984).
- A. Horovitz, A. R. Fersht, *J. Mol. Biol.* **214**, 613 (1990).
- A. Horovitz, L. Serrano, B. Avron, M. Bycroft, A. R. Fersht, *J. Mol. Biol.* **216**, 1031 (1990).
- P. Kopyrowski, A. Kubalski, *J. Membr. Biol.* **164**, 253 (1998).
- H. T. Kurata, D. Fedida, *Prog. Biophys. Mol. Biol.* **92**, 185 (2006).
- T. Nomura, M. Sokabe, K. Yoshimura, *Biophys. J.* **94**, 1638 (2008).
- S. B. Long, E. B. Campbell, R. MacKinnon, *Science* **309**, 903 (2005), published online 7 July 2005; 10.1126/science.1116270.
- S. B. Long, E. B. Campbell, R. MacKinnon, *Science* **309**, 897 (2005), published online 7 July 2005; 10.1126/science.1116269.
- S. B. Long, X. Tao, E. B. Campbell, R. MacKinnon, *Nature* **450**, 376 (2007).
- Y. Jiang *et al.*, *Nature* **423**, 33 (2003).
- O. Beckstein, M. S. Sansom, *Phys. Biol.* **3**, 147 (2006).
- G. N. Filatov, M. White, *Mol. Pharmacol.* **48**, 379 (1995).
- A. Miyazawa, Y. Fujiyoshi, N. Unwin, *Nature* **423**, 949 (2003).
- S. Miller *et al.*, *EMBO J.* **22**, 36 (2003).
- Our research was supported by the Wellcome Trust (grants GR077564MA and 040174), Medical Research Council (G0400277), Unilever (UK), and Biotechnology Biological Sciences Research Council (BBSRC) (BB/F003455/1). Structural biology used the facilities of the Scottish Structural Proteomics Facility funded by the Scottish Funding Council and BBSRC. We thank K. Johnson, T. Rasmussen, and F. Flett for their contributions to this work; D. Rees and R. Bass for advice on crystallization and for pre-release of x-ray intensities; and A. Leslie for a critical reading of the manuscript. Coordinates and data have been deposited in the Protein Data Bank (www.rcsb.org) with accession number 2zv5.

Supporting Online Material

www.sciencemag.org/cgi/content/full/321/5893/1179/DC1

Materials and Methods

Figs. S1 to S5

Table S1

References

17 April 2008; accepted 10 July 2008

10.1126/science.1159262

REPORTS

Polarized Gamma-Ray Emission from the Crab

A. J. Dean,¹ D. J. Clark,¹ J. B. Stephen,² V. A. McBride,¹ L. Bassani,² A. Bazzano,³ A. J. Bird,¹ A. B. Hill,¹ S. E. Shaw,¹ P. Ubertini³

Pulsar systems accelerate particles to immense energies. The detailed functioning of these engines is still poorly understood, but polarization measurements of high-energy radiation may allow us to locate where the particles are accelerated. We have detected polarized gamma rays from the vicinity of the Crab pulsar using data from the spectrometer on the International Gamma-Ray Astrophysics Laboratory satellite. Our results show polarization with an electric vector aligned with the spin axis of the neutron star, demonstrating that a substantial fraction of the high-energy electrons responsible for the polarized photons are produced in a highly ordered structure close to the pulsar.

The origin of the high-energy emission from rotation-powered pulsars and their associated pulsar wind nebulae (PWNs) is an unresolved problem. The observed pulsating radiation constitutes only a small fraction of the pulsar's spin-down energy losses; most of the energy is carried off in the form of a magnetized

relativistic pulsar wind. In a number of cases, including the Crab nebula, a highly collimated jet, thought to be aligned with the spin axis of the pulsar, and a circumstellar torus are also seen (*1–11*). The Crab is known to accelerate electrons and possibly other particles to extremely high energies, where observations in the gamma-ray domain can be used to trace them. Using imaging and polarization measurements of the unpulsed emission in the gamma-ray band, we showed that these energetic photons originate close to the pulsar.

The x-ray spectrum of the Crab varies on an angular scale of arc seconds throughout the (arc minute-sized) nebula (*12,13*), showing a gradual spectral softening from the inner pulsar region to the outer nebula, with a variation in photon index Γ from ~ 1.9 to ~ 3.0 (Γ is defined from the spectral relationship $F = KE^{-\Gamma}$ photons/cm²/s/keV, where K is a constant and E is the energy). This is consistent with particle injection from the pulsar in two different directions: the equatorial plane containing the torus and the axis of symmetry along the jet. Both these regions have spectral indices around 2.0, suggesting that the spectra of the electrons injected from the pulsar are similar in these two directions. The pulsed component is unambiguously attached to the rotating neutron star, although we have only scant ideas as to the detailed radiation processes. The origin of the nonpulsed emission, which constitutes $\geq 75\%$ of the emitted 0.1- to 1-MeV flux (*14*), is even less clear. Energetic electrons are capable of generating gamma rays through either the synchrotron or curvature radiation processes as they are accelerated within the magnetic field structure that permeates the PWN. However, because their radiative lifetimes are very short, they will necessarily radiate close to their acceleration zone and hence identify the source of injection.

¹School of Physics and Astronomy, University of Southampton, Southampton SO17 1BJ, UK. ²Istituto Nazionale di Astrofisica—Istituto di Astrofisica Spaziale e Fisica Cosmica (INAF-IASF), Via Piero Gobetti 101, 40129 Bologna, Italy. ³INAF-IASF, Via Fosso del Cavaliere 100, 00133 Roma, Italy.